Thermoacoustic Analysis of 3 K Thermal Buffer Tubes and Implications for Miniaturization of 1 Hz Pulse Tube Refrigerators

R. Snodgrass[1] **and J. Ullom**[1,2]

[1]National Institute of Standards and Technology, Boulder, Colorado, USA
[2]Department of Physics, University of Colorado Boulder, USA

ABSTRACT

The performance of pulse tube refrigerators is inextricably tied to the effectiveness of thermal buffer tubes, yet this component is rarely studied or analyzed in detail. In this work, we use thermoacoustic analysis to explain fundamental characteristics of 3 K to 300 K buffer tubes with and without Gedeon streaming. Our analysis is aimed towards the low-frequency, Gifford-McMahon-type (GM-type) pulse tube refrigerators that routinely reach extremely low temperatures, but which may be more susceptible to buffer tube losses due to relatively large boundary layers. Simplified expressions show that—in the absence of Gedeon streaming—buffer tube losses are too large to allow cooling power near 3 K. It is possible that the double-inlet configuration has been so critical for these very low temperatures because it enables Gedeon streaming, which is a very effective way to absorb buffer tube losses using the cooling power of the regenerator. As low-frequency pulse tube refrigerators operating near 3 K are miniaturized, a progressively larger proportion of this regenerator cooling capacity must be used to absorb losses from the progressively less-adiabatic buffer tube. Numerical tools suggest that the smallest state-of-the-art commercial coolers are already nearing miniaturization limits.

INTRODUCTION

The cooling power of a pulse tube refrigerator (PTR) is determined by the power flows through the components adjacent to the cold heat exchanger: the regenerator and thermal buffer tube (we prefer this name, since it unambiguously identifies the component instead of the whole refrigerator, also called a "pulse tube"). Although regenerators have seen extensive study in the field, buffer tubes have received relatively little attention. For example, we are aware of just a few studies that have experimentally measured power flows through buffer tubes [1, 2, 3]. Of these studies, only one [2] measured the total power flow and acoustic power flow through the tube, both of which are required to determine performance.

At NIST, we are particularly interested in the low-temperature ($\sim$3 K), low-frequency ($\sim$1 Hz) PTRs which are ubiquitously used to precool millikelvin refrigerators. It is unfortunate that buffer tubes have never been robustly studied in this class of refrigerator, since (due to relatively large boundary layers at 1 Hz) the buffer tube has the potential to be a major loss contributor. It is possible

Cryocoolers 24, edited by R.G. Ross, Jr., J.R. Raab and I.M. McKinley
© International Cryocooler Conference, Inc., Boulder, CO, 2026

that these buffer tubes have not received much study because their performance can be dramatically increased using the cooling power of regenerators. In the real-fluid regime, low-frequency regenerators have a very large cooling capacity [4]; this cooling can be used to absorb buffer tube loss if Gedeon streaming (steady flow) is directed from the regenerator towards the buffer tube. Although this strategy is effective, it does not come without cost. If buffer tube performance is poor then more Gedeon streaming is required to absorb losses, so less regenerator cooling is available for other system loads (such as precooling recirculating ^{3}He in dilution refrigerators).

The lack of previous buffer tube studies is also concerning with respect to the design tools that the field relies upon. Whether or not these numerical tools (e.g., Sage and DeltaEC) can accurately predict buffer tube performance is not known, since very few experimental measurements are available (none at low frequency and temperature). With these motivations in mind, we are undertaking a multi-year project to study buffer tubes. Combining thermoacoustic analysis, numerical results, and experimental observation, we hope to validate the design software that is used to model this component. We also hope to develop optimized methods for absorbing buffer tube loss. In this work, we begin with thermoacoustic analysis [5] to build fundamental understanding of the buffer tube. The implications of this analysis are significant; for example, we will show that GM-type PTRs would generally not be able to reach temperatures near 3 K without Gedeon streaming, and that Gedeon streaming is only viable as a loss absorption strategy for sufficiently large PTRs.

TOTAL POWER FLOW

The performance of a thermal buffer tube is characterized by how much power it transports from its cold end to its warm end. An ideal buffer tube is one that transports total power equal to the acoustic power; however, a more realistic quantification of performance begins with the total power flow $\dot{H}_2$ equation. For a generic thermoacoustic component, this is given by

$$\dot{H}_2 = \frac{1}{2}\mathrm{Re}[p_1\widetilde{U_1}f_{pu}] + \frac{\rho_m c_p |U_1|^2}{2\omega A_g} f_{uu}\frac{dT_m}{dx} - (A_g k + A_s k_s)\frac{dT_m}{dx} + \dot{N}mh, \tag{1}$$

where

$$f_{pu} = 1 - \frac{T_m \beta (f_\kappa - \widetilde{f_\nu})}{(1+\epsilon_s)(1+\sigma)(1-\widetilde{f_\nu})}, \tag{2}$$

and

$$f_{uu} = \frac{1}{(1-\sigma)|1-f_\nu|^2}\mathrm{Im}\left[\widetilde{f_\nu} + \frac{(f_\kappa - \widetilde{f_\nu})(1+\epsilon_s f_\nu/f_\kappa)}{(1+\epsilon_s)(1+\sigma)}\right]. \tag{3}$$

Total power flow includes any and all contributors to the First Law balance. In Eq. (1), the first term is pressure-induced (PI) enthalpy flow from the oscillating gas, the second is shuttle heat loss, the third is conduction, and the fourth is power carried by steady, non-oscillating flow. This sum does not change at different axial positions x along insulated components such as thermal buffer tubes: $d\dot{H}_2/dx = 0$. The subscript "2" shows that total power flow is second order in size; we neglect higher order terms because they are relatively small.

Enthalpy carried by the pressure p_1 and volumetric flow rate U_1 phasors is equal to the acoustic power $\dot{E}_2$ when $f_{pu} = 1$ (an ideal buffer tube) and is equal to 0 when $f_{pu} = 0$ (an ideal regenerator); realistic components fall somewhere in between, depending on the specifics of the boundary layers. Shuttle heat loss occurs through heat transfer between the gas in the boundary layer and the tube wall. It is proportional to the mean density ρ_m, the isobaric specific heat c_p, the square of the volumetric flow rate magnitude $|U_1|$, and the gradient of the mean gas temperature dT_m/dx. It is inversely proportional to the cross-sectional gas area A_g and the angular frequency ω. Like PI enthalpy flow, we have separated out a factor f_{uu} that modifies the shuttle heat loss and which is dependent upon the boundary layer. Thermal conduction takes place through both the gas ($A_g k$) and the solid ($A_s k_s$), and the power contributed from steady flow is the molar flow rate $\dot{N}$ multiplied by the molar mass m and specific enthalpy h.

Simplifying Eq. (2) and Eq. (3) requires knowledge of the Prandtl number σ, $f_{\nu,\kappa}$ (spatially-averaged, geometry-dependent thermoacoustic functions), and ϵ_s, the ratio of the fluid-to-solid thermal effusivities (also geometry dependent). At ambient temperature ϵ_s is small because $\sqrt{\rho c_p k}$ is much larger for stainless steel than for helium. We used the boundary layer approximations for f_ν and f_κ [5] and then simplified f_{pu} and f_{uu} using complex math. The following approximations are only valid for $\delta_{\nu,\kappa}/D \lesssim O(10^{-2})$, where D is the inner tube diameter. Assuming $\epsilon_s = 0$,

$$f_{pu} \approx 1 - \frac{\delta_\kappa}{D}\frac{4T_m\beta}{(1-\sqrt{\sigma})+i(1+\sqrt{\sigma})} \approx 1 - \frac{\delta_\kappa}{D}T_m\beta(0.23-2.2i) \quad (\sigma = 0.66), \tag{4}$$

where β is the thermal expansion coefficient, and

$$f_{uu} \approx \frac{2\delta_\nu}{D}\left[\frac{\sigma - 1/\sqrt{\sigma}}{(1-\sigma)(1+\sigma)}\right] \approx -\frac{2\delta_\nu}{D} \quad (\sigma = 0.66), \tag{5}$$

where the viscous penetration depth is $\delta_\nu = \sqrt{2\mu/\omega\rho_m}$ (dynamic viscosity μ) and the thermal penetration depth is $\delta_\kappa = \sqrt{2k/\omega\rho_m c_p}$ (thermal conductivity k). In Table 1 we calculated f_{pu}, f_{uu}, and ϵ_s exactly using the details given in [6] and the geometry and fluid properties pertinent to the Cryomech PT407, which is a convenient model cryocooler because we have studied it for many years. Although the simplified forms of f_{pu} and f_{uu} are useful for building intuition, Table 1 shows they are not exact in the systems of interest—a result of nonzero ϵ_s at 3 K and relatively large $\delta_{\nu,\kappa}/D$ at 300 K.

SIMPLIFIED BUFFER TUBE EFFECTIVENESS

Simplified expressions for buffer tube effectiveness η will be used to estimate what δ_ν/D is required to achieve $\eta \approx 1$; however, we caution that the following cannot be used to predict η to high accuracy. The equations are only valid for buffer tubes where PI enthalpy flow and shuttle heat loss are the only significant contributors to total power flow. Although a wide variety of loss mechanisms can reduce the effectiveness of real buffer tubes (e.g., isothermal-adiabatic transitions [7], Rayleigh streaming [8], turbulence, insufficient flow straightening, long gas strokes, and thermal conduction) those losses will not be considered in this work (although conduction is included in our DeltaEC results).

At 3 K and 1.25 MPa, real-fluid effects are large and $T_m\beta$ is only 0.08. The thermal penetration depth δ_κ is also very small (120 microns at 1.4 Hz) compared to the typical D of buffer tubes in

Table 1. Simplification or evaluation of parameters important for buffer tube analysis. At 3 K, 1.4 Hz, and 1.25 MPa, δ_ν is 92 microns. At 300 K δ_ν is about 16 times larger (1.5 mm). The symbol $i = \sqrt{-1}$.

Parameter	$\delta_{\nu,\kappa}/D \to 0$ $\epsilon_s = 0$, $\sigma = 0.66$	PT407 2nd buffer tube 3 K, 1.4 Hz	PT407 2nd buffer tube 300 K, 1.4 Hz
f_{pu}	$1 - \frac{\delta_\kappa}{D}T_m\beta(0.23-2.2i)$	$1.00 + 0.00i$	$0.93 + 0.23i$
f_{uu}	$-\frac{2\delta_\nu}{D}$	$-\frac{2\delta_\nu}{D}0.55$	$-\frac{2\delta_\nu}{D}1.23$
δ_ν/D		0.0052	0.086
δ_κ/D		0.0069	0.105
ϵ_s		$1.55 - 1.11i$	$0.005 - 0.002i$
$\rho_m c_p f_{uu}$ (J/m^{3}K)		-1730	-2180

low-frequency PTRs ($\gtrsim 1$ cm). The combination of these two effects causes f_{pu} to be very close to 1, so the PI enthalpy flow at the cold end is equal to the acoustic power flow at the cold end $\dot{E}_{2,c}$. The buffer tube effectiveness is then

$$\eta = \frac{\dot{H}_{2,c}}{\dot{E}_{2,c}} \approx \frac{1}{\dot{E}_{2,c}} \left[\frac{1}{2} \mathrm{Re}[p_1 \widetilde{U_1} f_{pu}] + \frac{\rho_m c_p |U_1|^2}{2\omega A_g} f_{uu} \frac{dT_m}{dx} \right]_c, \tag{6}$$

$$\approx 1 - \left[\frac{2\rho_m c_p L}{\gamma_i p_m \cos\theta} \frac{f_\epsilon}{f_{co}} \frac{\delta_\nu}{D} \frac{dT_m}{dx} \right]_c, \tag{7}$$

where θ is the angle by which U_1 leads p_1, subscript "c" denotes evaluation at the cold end, and L is the tube length. As expected, smaller δ_ν/D result in higher η. Equation (7) is an accurate estimate for η but contains multiple terms that are not easily estimated, so further simplification is useful. In Eq. (7) f_ϵ is a factor that accounts for nonzero ϵ_s and is important at very low temperatures. It is equal to 0.55 at the 3 K end of a PT407, but we'll estimate it as 1/2 in the following simplified expression. The compliance factor f_{co} is

$$f_{co} \equiv \frac{\omega V |p_1|}{\gamma_i p_m |U_{1,c}|}. \tag{8}$$

If a buffer tube of volume V were a closed-end tube filled with an ideal gas at mean pressure p_m, with ideal-gas specific heat ratio γ_i, and were compressed at angular frequency ω, a cold-end volumetric flow rate amplitude $|U_{1,c}|$ would generate pressure amplitude $|p_1|$ in the tube. In other words, $f_{co} = 1$ corresponds to the pressures and flows at the entrance of a closed-end tube filled with an ideal gas. Compliance factors greater than 1 are generally only possible in double-inlet PTRs (DIPTRs) [9], as larger $|p_1|$ can be generated than with $|U_{1,c}|$ alone because the bypass flow assists with compression. A phasor diagram may provide a more intuitive understanding of f_{co} (bottom-middle of Fig. 1).

Let us proceed by considering the buffer tube of an OPTR since it simplifies analysis ($f_{co} \approx \sin\theta_c$) and is as effective or more effective than DIPTR buffer tubes (as we will show later). In this work, the distinction between an OPTR and DIPTR is that the phasor $U_{1,w}$ is estimated as real for an OPTR ($\theta_w = 0°$) but in the fourth quadrant for a DIPTR (Fig. 1). Assuming a modest cold end phase $\theta_c = 45°$ and a linear temperature profile (considered in the next section), then a rough approximation for η is

$$\eta \approx 1 - \left[\frac{2\rho_m c_p \Delta T}{\gamma_i p_m} \frac{\delta_\nu}{D} \right]_c. \tag{9}$$

Using the buffer tube geometry of a PT407 ($D \approx 1.76$ cm), η is only expected to be 0.55. This is unacceptably low: for there to be nonzero cooling the power flow through the buffer tube must be greater than the power flow through the regenerator. In low-frequency PTRs operating near 3 K, the regenerator power flow depends only upon real-fluid and finite-heat capacity losses, which are simple functions of temperature [4]. Assuming gadolinium oxysulfide as the cold-end material, the regenerator power flow at 1.4 Hz and 3 K will be close to $0.95\dot{E}_{2,c}$. To increase the buffer tube effectiveness up to 0.95 in this example would require a tube with a diameter 9 times larger (16 cm) or a temperature gradient 9 times smaller than $\Delta T/L$. Effectiveness close to 1 is desirable in real PTRs since regenerator losses cannot be mitigated; for $\eta = 0.99$, a tube diameter of 79 cm or a temperature gradient 45 times smaller than $\Delta T/L$ is required! As we will show later, decreasing $dT_m/dx|_c$ is the method by which commercial PTRs achieve sufficiently high η.

BUFFER TUBE TEMPERATURE PROFILES

Low compliance factor

Now we consider the shape of buffer tube temperature profiles in the absence of Gedeon streaming. Let us first restrict our analysis to buffer tubes with low compliance factors ($f_{co} \ll 1$).

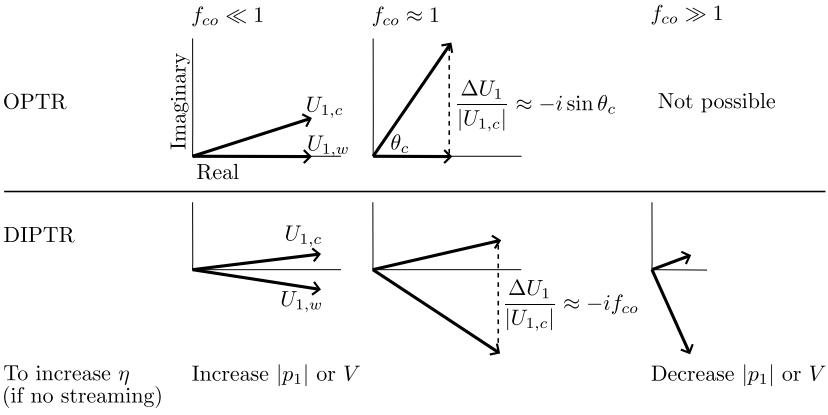

Figure 1. Typical phasor diagrams for orifice PTRs (OPTRs) and double-inlet PTRs (DIPTRs) at different compliance factors f_{co}. By convention p_1 is real and does not change end to end.

Low f_{co} buffer tubes are unusual since gas compliance cannot normally be ignored, but this analysis provides a good foundation for $f_{co} \gtrsim 1$. With $f_{co} \ll 1$, the imaginary part of U_1 changes little (relative to $|U_{1,c}|$) from one end of the tube to the other. If we also restrict our analysis to small $\delta_{\nu,\kappa}/D$, then good approximations are that $\mathrm{Re}[U_1]$ changes little through the tube and $f_{pu} \approx 1$. Under these conditions the PI enthalpy flow $\mathrm{Re}[p_1 \widetilde{U_1} f_{pu}]/2$ is nearly the same at both ends, so that (neglecting conduction) shuttle heat loss must also be approximately equal at both ends:

$$\left[\frac{\rho_m c_p |U_1|^2}{2\omega A_g} f_{uu} \frac{dT_m}{dx}\right]_c \approx \left[\frac{\rho_m c_p |U_1|^2}{2\omega A_g} f_{uu} \frac{dT_m}{dx}\right]_w, \tag{10}$$

where subscript "w" denotes evaluation at the warm end. The above gives the ratio of the temperature gradients:

$$\frac{dT_m/dx|_w}{dT_m/dx|_c} \approx \frac{[\rho_m c_p f_{uu} |U_1|^2]_c}{[\rho_m c_p f_{uu} |U_1|^2]_w}. \tag{11}$$

As shown in Table 1, $\rho_m c_p f_{uu}$ is not very different at the 3 K and 300 K ends. This is perhaps a surprising result: even though the boundary layers at 3 K are about 16 times smaller than they are at 300 K, shuttle heat loss can be as substantial at the 3 K end (for the same flow rate and temperature gradient) because the dense helium there carries more heat per unit volume compared to the relatively thick (but low density) boundary layer at the warm end.

Since we have limited our analysis to scenarios where the real and imaginary parts of U_1 are not changing significantly, Eq. (11) shows that the temperature gradients at the two ends would be nearly equivalent and the profile linear; such behavior may occur for both OPTR and DIPTR configurations so long as f_{co} and $\delta_{\nu,\kappa}/D$ are small. However, if we further restrict our analysis to only OPTRs, then $|U_{1,w}|/|U_{1,c}| \approx \cos\theta_c$. Still assuming similar $\rho_m c_p f_{uu}$ at both ends, the ratio of the temperature gradients becomes

$$\frac{dT_m/dx|_w}{dT_m/dx|_c} \approx \frac{1}{\cos^2\theta_c}. \tag{12}$$

High compliance factor

There are two changes to consider when the compliance factor approaches or exceeds 1. The first change is that the ratio $|U_{1,c}|/|U_{1,w}| \neq 1$. In an OPTR this ratio can be greater than 1 and in a DIPTR this ratio may tend to be much less than 1 (Fig. 1). If the PI enthalpy flow at the two ends is equivalent, then Eq. (11) shows OPTRs will tend to produce concave up temperature profiles and DIPTRs will tend to produce concave down temperature profiles.

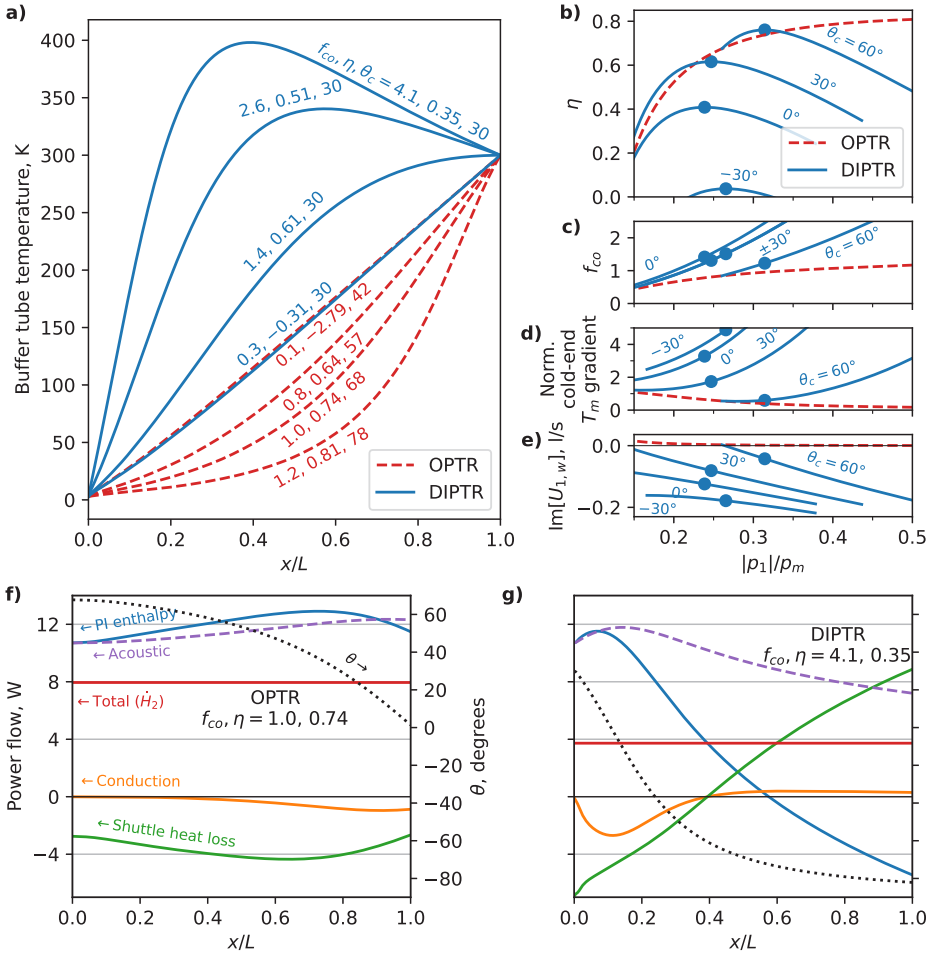

Figure 2. a) Example temperature profiles for OPTRs and DIPTRs, showing increased concavity for higher compliance factors. b-e) As a function of the pressure amplitude normalized by the mean pressure: b) buffer tube effectiveness, c) compliance factor, d) cold-end temperature gradient normalized by mean temperature gradient, and e) imaginary part of the volumetric flow rate at the warm end. Markers indicate effectiveness maxima. f) Components of the total power flow (excludes acoustic) and phase for one of the OPTR profiles shown in a). g) Components of the total power flow (excludes acoustic) and phase for one of the DIPTR profiles shown in a). $x/L = 0$ is the cold end and $x/L = 1$ is the warm end.

The second change to consider is that the PI enthalpy flows at the two ends may not be equivalent. This occurs in buffer tubes when the warm-end penetration depths become significant fractions of D; for example, in the PT407 second stage buffer tube $\delta_{\nu,w}/D$ is 0.086 and the imaginary part of $f_{pu,w}$ is 0.23 (important because the product of Im$[f_{pu}]$ and Im$[\widetilde{U_1}]$ creates real changes to the PI enthalpy flow). The PI enthalpy flow increases from cold to warm end if Im$[U_{1,w}]$ is large and positive (unusual) but decreases from cold to warm end if Im$[U_{1,w}]$ is large and negative (common

Table 2. Characteristics of 3 K to 300 K thin-walled buffer tubes in the absence of Gedeon streaming.

Type	$f_{co} \ll 1$ profile	$f_{co} \approx 1$ profile	$f_{co} \gg 1$ profile	η as $\lvert p_1 \rvert$ increases at fixed $\dot{E}_{2,c}$
OPTR	Linear	Concave up	Not possible	Increases
DIPTR	Linear	Concave down	Concave down, max $> T_w$	Increases until $f_{co} \approx 1$, then decreases

in DIPTRs). The change in PI enthalpy flow from cold to warm end is

$$\Delta \dot{H}_{pu} = \left[\frac{1}{2}\mathrm{Re}[p_1 \widetilde{U_1 f_{pu}}]\right]_w - \dot{E}_{2,c} = \frac{|p_1|}{2}\left[\mathrm{Re}[U_1]\mathrm{Re}[f_{pu}] + \mathrm{Im}[U_1]\mathrm{Im}[f_{pu}]\right]_w - \dot{E}_{2,c}, \tag{13}$$

$$\approx \frac{|p_1|}{2}\left[\mathrm{Im}[U_1]\mathrm{Im}[f_{pu}]\right]_w. \tag{14}$$

To arrive at Eq. (14) we assumed that $\mathrm{Re}[U_{1,w}] \approx \mathrm{Re}[U_{1,c}]$ and $\mathrm{Re}[f_{pu}] \approx 1$ (this latter approximation seems to be fair even when the penetration depths are significant, see Table 1).

In OPTRs the flow at the warm end of the buffer tube is approximately real, and Eq. (14) shows that the change in PI enthalpy would be approximately zero. In DIPTRs, however, the imaginary component of $U_{1,w}$ is often large and negative, so the PI enthalpy flow will be lower at the warm end than at the cold end (we will call this the "PI enthalpy deficit" going forward). To conserve total power flow, shuttle heat loss (typically negative) must grow more negative at the cold end, causing $dT_m/dx|_c$ to rotate CCW and $dT_m/dx|_w$ CW. At very large f_{co}, $dT_m/dx|_w$ can even change from positive to negative, so that the maximum temperature of the tube is greater than T_w.

The above behavior is summarized in Table 2 and confirmed by numerical models made in DeltaEC (Fig. 2a). All models shown in this work consider a fixed buffer tube geometry (from the second stage of the PT407) and fixed $\dot{E}_{2,c} = 10.7$ W (estimated using regenerator physics [4]) unless specified otherwise.

EFFECTIVENESS AND PRESSURE AMPLITUDE

Do high or low pressure amplitudes produce higher buffer tube effectiveness? The answer depends on whether $\theta_w \approx 0°$ (as in an OPTR) or $\theta_w < 0°$ (as in an DIPTR). Let us first consider the expected change in η for an OPTR buffer tube as we increase the pressure amplitude (or f_{co}, since it is proportional to $|p_1|$) with fixed $\dot{E}_{2,c}$. Effectiveness will be increased if the bracketed term in Eq. (7) decreases. Considering the same tube geometry, frequency, and cold-end temperature, the only parameters in the bracketed term that change are $\cos\theta$, f_{co}, and dT_m/dx. A decrease of the product $[(\cos\theta f_{co})^{-1} dT_m/dx]_c$ will produce higher η. Although f_{co} can be slightly greater than $\sin\theta_c$ because helium at very low temperatures is less compliant than an ideal gas, we assume $f_{co} \approx \sin\theta_c$ here in order to build intuition.

An estimate for $dT_m/dx|_c$ is made using Eq. (12), which is valid for OPTRs with small penetration depths. Since a continuous, monotonic profile between T_c and T_w should form for $T_c \approx 3$ K, we will also assume that the product of the gradients is fixed at $(\Delta T/L)^2$, i.e., if the cold-end gradient halves then the warm-end gradient doubles. Therefore, $dT_m/dx|_c \propto \cos\theta_c$ and $[(\cos\theta f_{co})^{-1} dT_m/dx]_c \propto 1/\sin\theta_c$, showing that the buffer tube effectiveness should increase in OPTRs with increasing θ_c or $|p_1|$. This is the same behavior observed using DeltaEC (Fig. 2b).

Although we have shown mathematically that low f_{co} or $|p_1|$ leads to lower η in OPTRs, what is the physical explanation? Acoustic power is generated by the product of pressure and flow rate oscillations. Low f_{co} means the acoustic power is generated less by p_1 and more by U_1, the flow responsible for shuttle heat loss (second term of Eq. (1)). Considering only the buffer tube effectiveness, the same amount of acoustic power would be better generated by increasing p_1 and decreasing U_1. We have already established that increasing f_{co} (or p_1) causes $dT_m/dx|_c$ to decrease in OPTRs, so both of these effects contribute to higher η at higher $|p_1|$.

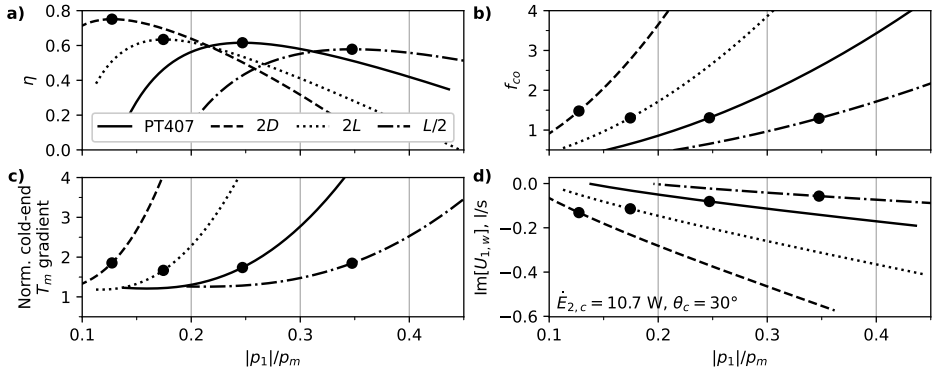

Figure 3. a) Effectiveness, b) compliance factor, c) cold-end temperature gradient normalized by the mean, and d) the imaginary part of the flow rate at the warm end as a function of the pressure amplitude normalized by the mean pressure. Solid lines are for the PT407 buffer tube geometry while the others are for modified diameters or lengths (see legend). Markers indicate effectiveness maxima.

The behavior is different in DIPTRs: higher $|p_1|$ can—but does not always—increase η. While increasing $|p_1|$ at fixed $\dot{E}_{2,c}$ decreases the amount of flow that participates in shuttle heat loss, the temperature gradient can grow very steep at $f_{co} \gg 1$ (Fig. 2a,d). It is this tradeoff that produces an optimal $|p_1|$ in DIPTR buffer tubes; using DeltaEC, we find that this optimum occurs at $f_{co} \approx 1$ or 1.5 (Fig. 2c) if there is no streaming. As discussed previously, the mechanism for the growing temperature gradient is the PI enthalpy deficit at the warm end (as shown in Fig. 2g).

In a DIPTR, the phase of $U_{1,c}$ can be either positive or negative. For positive θ_c, the buffer tube is compressed by gas from both the bypass and the cold end of the regenerator [10]. Alternatively, negative θ_c corresponds to very large bypass flows which compress all the gas in the buffer tube (and some portion of the regenerator). Figure 2b shows much higher η for more positive θ_c. This is explained not by differences in the flow rate (identical for our $30°$ and $-30°$ results) but by differences in the temperature gradient; for example, at low pressure amplitudes $dT_m/dx|_c$ is roughly twice as high for $\theta_c = -30°$ as for $\theta_c = 30°$ (Fig. 2d). Elevated $dT_m/dx|_c$ is explained by larger, negative Im$[U_{1,w}]$ (Fig. 2e) and the resultant warm-end, PI enthalpy deficit (Eq. (14)).

Because too little or too much compliance leads to non-optimal η in a DIPTR, the tube volume also impacts the optimal pressure amplitude. Figure 3a shows that increasing V (either by increasing D or L) shifts the optimal $|p_1|/p_m$ lower, while decreasing the tube volume shifts it higher. Optimal f_{co} is between 1 and 1.5 for any of the tube geometries (Fig. 3b). Shuttle heat loss is exacerbated at larger f_{co} because of large $dT_m/dx|_c$ (Fig. 3c) that result from negative Im$[U_{1,w}]$ (Fig. 3d).

Although these DIPTR results suggest a need to carefully optimize $|p_1|$ or V, this complexity can be avoided by suppressing $dT_m/dx|_c$ with streaming, which is discussed next. We reiterate that the analysis in these preceding sections assumed no streaming and a PI enthalpy flow at the cold end equal to acoustic power; analysis may not be valid if these assumptions are not met.

3 K COMMERCIAL DIPTRS ARE ENABLED BY GEDEON STREAMING

We previously established that $\eta \to 1$ is required to overcome regenerator losses and produce cooling when $T_c \approx 3$ K. Our analysis suggested a 1.4 Hz, 3 K to 300 K buffer tube of size similar to those in commercial coolers is not possible because shuttle heat loss is too large relative to $\dot{E}_{2,c}$. However, Gedeon streaming [11] (or steady flow) can be used to drastically increase η. When this streaming is directed from the cold to the warm end of the buffer tube, the cooling power of the regenerator can be used to decrease $dT_m/dx|_c$ and therefore decrease both shuttle heat loss and conduction at the cold end.

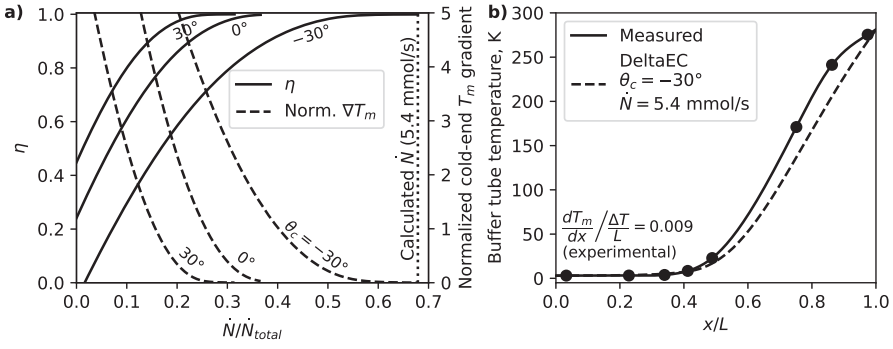

Figure 4. a) Effectiveness and normalized temperature gradient as a function of streaming. b) The measured buffer tube temperature profile for a PT407 (solid) compared to one example DeltaEC result (dashed). While streaming is calculated from measurements, we do not have a good estimate for cold-end phase.

Figure 4a quantifies the above behavior. In this figure, we used previous measurements from a PT407 to estimate η as a function of Gedeon streaming $\dot{N}$ compared to the total regenerator cooling (also expressed as a molar flow rate $\dot{N}_{total}$). This total includes both the estimated amount of streaming through the regenerator and the capacity of the regenerator to support additional streaming until all regenerator cooling is exhausted. The latter part was studied in depth in [4] and the former was estimated originally by an experiment in [12] and refined in [4]. The required $\dot{N}$ to bring η very close to 1 is about $0.6\dot{N}_{total}$ if the cold-end phase is $-30°$, but is only about $0.3\dot{N}_{total}$ if the cold-end phase is $30°$. This is an important observation: although the DIPTR geometry enables Gedeon streaming (which may be used to increase η) it is also used to decrease θ_c. In tubes with non-negligible boundary layers at the warm end, lower θ_c decreases η (Fig. 2b) because of the increases to $dT_m/dx|_c$ from the PI enthalpy deficit.

Unfortunately, our previous measurements do not enable us to estimate θ_c. Nevertheless, in Fig. 4b we compare the experimentally measured buffer tube profile [12] to a profile from DeltaEC with the estimated $\dot{N}$ (5.4 mmol/s). The profiles are in reasonable agreement if θ_c is close to $-30°$. We do not suggest that θ_c must equal $-30°$; however, we include this result to show that our estimates for $\dot{E}_{2,c}$ and $\dot{N}$—although not yet confirmed with direct measurements—may still be reasonable. There are other reasons why the experimental and DeltaEC results may disagree; for example, there could be buffer tube losses present that are not captured in the DeltaEC model, and the waveforms in this refrigerator are not the low-amplitude sinusoidal waves that DeltaEC assumes (flows were measured in [13]).

The length of the PT407's second stage buffer tube appears close to optimal. Figure 5a shows that increasing L would change the streaming required to reach high η very little, while decreasing L could drastically increase the required streaming. Although we previously found that f_{co} between about 1 and 1.5 results in the highest η for a DIPTR, higher f_{co} appears favorable once streaming is introduced. For the PT407 f_{co} is likely between 3.5 and 4 (Fig. 5a), while f_{co} around 1 or 1.5 would require significantly more streaming. This could be explained by the following: in the absence of streaming $f_{co} \gg 1$ creates poor effectiveness through $dT_m/dx|_c \gg \Delta T/L$; however, with Gedeon streaming $dT_m/dx|_c$ is suppressed, and larger f_{co} is beneficial because smaller $U_{1,c}$ is required to generate $\dot{E}_{2,c}$.

LIMITS TO MINIATURIZATION

Smaller 1 Hz PTRs are of interest for a variety of low-temperature applications. However, as the buffer tube diameter shrinks and the boundary layer thicknesses remain fixed, the buffer tube will become progressively less effective. In the limit of $\delta_{\nu,\kappa}/D \to 0.5$, the component no longer acts like a thermal buffer tube but instead a thermoacoustic stack.

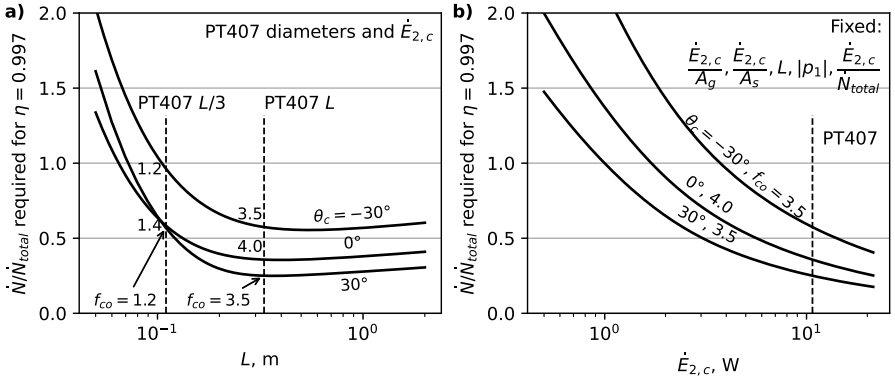

Figure 5. Required Gedeon streaming for high buffer tube effectiveness when a) the buffer tube length is changed or b) when the cryocooler is scaled down in size (quantified here by cold-end acoustic power). When $\dot{N}/\dot{N}_{total} = 1$ there is just enough regenerator cooling to achieve high buffer tube effectiveness, while $\dot{N}/\dot{N}_{total} < 1$ means there would be regenerator cooling available for other uses as well.

Now we use DeltaEC to estimate how small these GM-type 3 K PTRs can be made if they are simply scaled down in size. We start with the parameters of the PT407 and decrease the the acoustic power flow (proportional to the cooling power if there are no buffer tube losses), keeping $\dot{E}_{2,c}/A_g$ and $\dot{E}_{2,c}/A_s$ fixed. Figure 5b shows that relatively more Gedeon streaming is required to keep η high as the acoustic power is decreased. In Fig. 5b we also assumed that $\dot{E}_{2,c}/\dot{N}_{total}$ is fixed—likely a fair assumption since the available regenerator cooling is determined by the difference of the temperature-dependent power flow terms at the two ends of the regenerator, which are proportional to $\dot{E}_{2,c}$ [4, 14]. Again we observe that the required streaming for high η is very sensitive to the cold-end phase. For $\theta_c = 30°$, there is just enough regenerator cooling available for $D = 0.54$ cm and $\dot{E}_{2,c} = 1$ W, about a factor of 10 smaller than the PT407, which consumes 6 kW or 7 kW of electricity to produce 700 mW of cooling at 4.2 K.

Our very simplified scaling analysis shows a cooler that consumes about 600 W to 700 W of electricity while providing about 70 mW of cooling at 4.2 K may be possible. Although other losses may prevent such a simple miniaturization of current commercial systems, this is the scale at which buffer tube losses would start to overwhelm available regenerator cooling assuming fixed $\dot{E}_{2,c}/A_g$. Smaller 1.4 Hz DIPTRs do not appear possible unless new strategies to enhance buffer tube effectiveness are developed.

CONCLUSION

The DIPTR configuration is widely recognized for decreasing the phase between flow and pressure at the cold end of PTRs. Lower phase usually increases regenerator performance, but it has the negative effect of increasing shuttle heat loss in the buffer tube. These increased losses may not impact the cooling available at the cold end of 3 K PTRs because they can be substantially (perhaps completely) absorbed by Gedeon streaming, which is enabled by the DIPTR's toroidal geometry. Other studies have rightly attributed more cooling power in DIPTRs to Gedeon streaming [15, 16], but we are not aware of any that have clearly connected buffer tube performance with streaming and regenerator cooling. As we have demonstrated here, shuttle heat loss in a 3 K to 300 K buffer tube would be large enough to completely overwhelm gross cooling power in a typical commercial PTR; Gedeon streaming (in effect) utilizes the excess cooling power of the regenerator to absorb those buffer tube losses. Optimized buffer tube design is still important because then regenerator cooling may be available for other uses.

A scaling analysis shows that buffer tube losses limit the simple miniaturization of GM-type PTRs (i.e., scaling down current designs is only feasible for slightly smaller refrigerators). As tube diameter is decreased, the buffer tube's adiabaticity diminishes and the cooling power of the regenerator is—at some point—no longer sufficient to absorb buffer tube losses. Our estimated limit ($\sim$70 mW at 4.2 K with 600 W or 700 W of electricity input) is close to the smallest commercially-available, low-frequency PTR (Cryomech PT205: $\sim$180 mW at 4.2 K with $\sim$1.2 kW of electricity input). This miniaturization limit appears to be very sensitive to the cold-end phase.

ACKNOWLEDGMENTS

Manuscript is a contribution of NIST, and not subject to copyright. Certain equipment, instruments, or materials are identified in this paper in order to specify the experimental procedure adequately. Such identification is not intended to imply recommendation or endorsement by NIST, nor is it intended to imply that the materials or equipment identified are necessarily the best available for the purpose. We acknowledge guidance and advice on the topic of this manuscript from Vincent Kotsubo, Gregory Swift, and Ray Radebaugh. This document has not been peer reviewed but has been cleared by NIST for release.

REFERENCES

1. Hagiwara, Y, Nara, K, Ito, S, and Saito, T, "Temperature measurement in pulse tube with Rayleigh scattering and computation of enthalpy flow," *Cryogenics* 39.5 (1999), pp. 425–434.
2. Rawlins, W., Radebaugh, R., Bradley, P. E., and Timmerhaus, K. D., "Energy Flows in an Orifice Pulse Tube Refrigerator," *Advances in Cryogenic Engineering*, Springer US (1994), pp. 1449–1456.
3. Jeong, S., Nam, K., Kim, M. G., Chang, H. M., and Jeong, E. S., "Experimental Study of the Heat Transfer in Pulse Tubes," *Cryocoolers 11*, Springer US (2002), pp. 345–351.
4. Snodgrass, R., Swift, G., Ullom, J., and Backhaus, S., "Intermediate cooling from pulse tube refrigerator regenerators operating in the real-fluid regime," *Cryogenics* 132 (2023), p. 103 685.
5. Swift, G. W., *Thermoacoustics: A Unifying Perspective for Some Engines and Refrigerators*, Springer International Publishing (2017).
6. Ward, B., Clark, J., and Swift, G., *Users Guide for DeltaEC*, 2026. [Online]. Available: `https://www.losalamosthermoacoustics.org/deltaec.html`
7. Kittel, P, "Enthalpy Flow Transition Losses in Regenerative Cryocoolers," *Cryocoolers 7* (1993), pp. 1145–1156.
8. Olson, J. R. and Swift, G. W., "Acoustic streaming in pulse tube refrigerators: tapered pulse tubes," *Cryogenics* 37.12 (1997), pp. 769–776.
9. Zhu, S., Wu, P., and Chen, Z., "Double inlet pulse tube refrigerators: an important improvement," *Cryogenics* 30.6 (1990), pp. 514–520.
10. Kotsubo, V., "Real and Reactive Flows in Regenerative Cryocoolers," *Cryocoolers 21* (2021), pp. 245–253.
11. Gedeon, D., "DC Gas Flows in Stirling and Pulse Tube Cryocoolers," *Cryocoolers 9* (1997), pp. 385–392.
12. Snodgrass, R., Kotsubo, V., Ullom, J., and Backhaus, S., "Leveraging Real Fluid Effects as a Tool for Power Flow Measurements in 4 K Cryocooler Regenerators," *Cryocoolers 21* (2021), pp. 315–324.
13. Snodgrass, R., Kotsubo, V., Höhne, J., and Ullom, J., "Low-frequency cryocoolers are compressed inefficiently," *Physical Review Applied* 25.3 (2026), p. L031001.
14. Snodgrass, R., Ullom, J., and Backhaus, S., "Role of Non-Temperature-Gradient Power Flow Terms in Low-Temperature Regenerators," *Cryocoolers 22* (2022), pp. 291–302.
15. Wang, C., Thummes, G., and Heiden, C., "Control of DC gas flow in a single-stage double-inlet pulse tube cooler," *Cryogenics* 38.8 (1998), pp. 843–847.
16. Wang, C., Thummes, G., and Heiden, C., "Effects of DC gas flow on performance of two-stage 4K pulse tube coolers," *Cryogenics* 38.6 (1998), pp. 689–695.